

The Effect of Voids on Flexural Capacity of Reinforced Concrete Slabs

Firat Kıpçak^{1*}, Barış Erdil², Mucip Tapan², Abdulhalim Karaşin³

¹ Department of Construction, Van Vocational School, Van Yuzuncu Yil University, 65080, Campus Van, Türkiye

² Department of Civil Engineering, Faculty of Engineering, Van Yuzuncu Yil University, 65080, Campus Van, Türkiye

³ Department of Civil Engineering, Faculty of Engineering, Dicle University, 21280, Diyarbakır, Türkiye

* Corresponding author, e-mail: firatkipcak@yyu.edu.tr

Received: 03 February 2023, Accepted: 01 June 2023, Published online: 20 June 2023

Abstract

The voided reinforced concrete slab system is mainly produced with polyester foam placed mostly at the bottom of the slab. The aim of the voids is to reduce the weight of the slab. In this paper behavior of the voided reinforced concrete slabs in which voids placed at the mid-height of the slab cross-section, is examined analytically. A series of models were created to come up with a lightweight slab. Two distinct slab models were analyzed using the ABAQUS software. In the first group, slabs had three layers, in which bottom and top layers were of solid reinforced concrete, but the mid layer was of voided unreinforced concrete. In the second layer, in order to increase the contact between top and bottom layers of the slab, crossties were utilized, and the mid layer was reinforced accordingly. Since all the layers were 5 cm thick, the total thickness of the slabs were 15 cm. Slabs were 100 cm wide and 200 cm long. They were simulated the three-point bending test. Concrete damaged plasticity material model (CDPM) for concrete and elastoplastic material model for steel was selected. From the results it was found that moment capacity decreased with the increase in the volume of the voids. There was a sudden decrease in strength after reaching the yield strength in voided slab without a crosstie. In addition, crossties enabled the reduction of the weight of the slabs without significant decrease in moment capacity.

Keywords

composite slab, crosstie, flexural analysis, one-way slab, polystyrene foam, voided slab

1 Introduction

Earthquake load is directly related to the weight of the building, i.e., higher weight corresponds to the higher seismic forces. Weight of the building is affected from the slab weight directly since slabs are stated to consist almost 40–60% of the dead load in a typical reinforced concrete residential building [1, 2]. Conventional and heavy slabs may create additional problems in large buildings or high-rise buildings. One of the problems is that the building needs large beams and large vertical members to carry such heavy slabs and those large load carrying members further increase the dead load of the building which then end up with increased cost [1, 3]. Therefore, in order to create cost effective and safe buildings, the weight of the building should be reduced. A light-weight building having sufficient stiffness, ductility and load carrying capacity is the target to be sought by many researchers.

As mentioned above, since the contribution of the slabs to the total weight is high, reducing the weight of the slab

will significantly decrease the weight of the building. This can be achieved either by using lightweight concrete or introducing voids in the slabs.

Lightweight aggregates are used to produce lightweight concrete. The aggregate varies from natural materials like pumice, shale, scoria etc., to artificial materials such as waste tires, crushed bricks etc. Lightweight aggregates, if used in proper mix ratios, can enhance the compressive strength of the concrete [4–7]. However, not only strength is important, but also stiffness and ductility should be questioned because beams and slabs are under continuous bending. Studies revealed that lightweight concrete slabs showed almost the same behavior as the normal weight concrete but because of the reduction in stiffness and ductility they exhibit large deflection and less ductility. Besides, moment capacity is stated to be related to the tensile reinforcement rather than the effect of the weight or strength of the concrete [8–16]. In order to increase the

stiffness properties of the flexural members, high-strength lightweight concretes were utilized, and good performances were reported [9, 17].

The other technique to reduce the weight is to create intentional voids in the cross-section of the slabs. Several void shapes; donut [18–20], spherical [21–28], cuboid [1 and 28–31], ellipsoidal [27, 32, 33], flat void [21] etc. were used and several configurations (discrete void, continuous void etc.) were studied. The voids may either be filled with a lightweight material namely polystyrene foam [23, 34, 35, 36] which is common in slab constructions or left unfilled. If the void was not filled, then the void former may be manufactured using a lightweight material like plastic, recycled plastic (polyethylene high-density, PE-HD or polypropylene, PP) [19, 21, 22, 24] or cardboard [37].

Although several different void configurations were studied, results seemed to be common. In general, following conclusions were drawn:

- Voids decrease the flexural stiffness. The reduction may be up to 50% [28]. Therefore, actual stiffness was recommended to be taken into account while calculating the deflections.
- Behavior of voided slabs was similar to the solid ones; crack formation was not different thus yield line theory can be applied. A well-pronounced failure mechanism was observed indicating the yielding of tension reinforcements and crushing of concrete at the compression side.
- Maximum load carried by the voided slabs were similar to the load carried by the solid ones. Slight differences were reported.
- Discontinuities created by the voids in the slab section, stress concentration occurs at the edges of the voids. This was reported to negatively affect the capacity and the behavior [34, 35, 38, 39, 40].

In addition to the above findings, some restrictions were also stated [21]:

- Voids reduce the concrete thickness at the top and bottom of the slab resulting in a reduced compression zone under bending. This may lead to a brittle behavior.
- Since the concrete area is reduced, shear resistance may reduce.
- Voids should be carefully placed in the slab because solid zones may be needed in case of punching.
- Reducing the concrete thickness at the compression zone may lead to a local punching.

- Construction joints should be carefully treated if they coincide with the voids which reduce the shear area.

It can be said that introducing voids results in a reduced ductility, stiffness and shear capacities. In order to compensate this reduction those slabs are made thicker than solid slabs.

In addition to the voids, behavior of slabs is affected from several factors: material, thickness of the slab, ratio of tension and compression reinforcements, number-dimension and amount of the voids in the section and cross-ties. Many studies dealt with the effect of void ratio [1, 34, 35, 41] and in general it was found that moment and shear capacities of the slab decreases, and the displacements increases due to the increase in the void ratio. Besides, in the study of Allawi and Jabir [42], slab moment capacities increased and displacement values decreased as a result of the use of cross-ties in voided slabs. Wang et al. [43], has observed that the slab strength and displacement capacities increase when steel fiber reinforced concrete is used.

In this paper, effect of the amount of the cuboid voids placed at the mid-height of the slabs on the behavior was examined analytically. A series of models were created to come up with a lightweight slab having great moment capacity. Two distinct slab models were designed. In the first group, slabs had three layers, in which bottom and top layers were of solid reinforced concrete, but the mid layer was of voided unreinforced concrete. In the second group, in order to increase the contact between top and bottom layers of the slab, cross-ties were utilized, and the mid layer was reinforced accordingly. The voids were filled with polystyrene foam and in order to attain the lighter slab having better structural performance. The aim of this study was targeted to understand the effect of the following on slab behavior:

- void ratio,
- void configuration,
- use of cross-tie.

2 Materials and method

2.1 Slab models and materials

A total of 10 slabs grouped into two (5 slabs in each group) and having $200 \times 100 \times 15$ cm dimensions were designed. Concrete strength was 30 MPa. Group S-N slabs had three layers; bottom and top layers were of reinforced concrete (with 5 cm thickness) whose reinforcements were placed according to TS500-2000 [44], the mid-layer (again 5 cm thick) was of concrete without reinforcement and voids

filled with polystyrene were placed in this layer in order to reduce the weight of the slab (Fig. 1 and Fig. 2). According to TS500-2000 [44], a minimum reinforcement ratio of 0.002 is used in both directions in the slab. In this context, in order to keep the rebar spacing constant, it is taken as 0.0026 (corresponding to $f_6/75$, diameter/distance in mm) equal in all both directions. Void ratio was the main variable in this group. Slab S-N-0 had no voids and was the control slab, however, Slab S-N-10 had a 10% void ratio whereas it was 13.3% in Slab S-N-13. Remaining slabs, S-N-16 and S-N-20 had 16.7 and 20% void ratio, respectively. Weight of S-N-0 was 7.5 kN and it reduces continuously up to 5.59 kN in S-N-20. Concrete width between the voids reduced from 12 cm to 6 cm in S-N-10 and S-N-20, respectively. Less shear area was provided in S-N-20. In 3d drawings, the gray color represents the concrete and the red color represents the void. The enlargement of the red layer indicates that the void is increasing (Fig. 1 and Fig. 2).

In the second group (Group S-C), the same slabs as in Group S-N were manufactured (Fig. 3). Therefore, the same dimensions, same void ratio and same reinforcement ratio were utilized in this group. The only difference was the crosssties which were aimed to compensate for the strength loss to be caused by the voids. Crosssties were of S-shape and extended from bottom concrete to the top concrete and embedded into the concrete with a hook

length of 6 cm (Fig. 4). Ratio of crosssties were kept constant in all the slabs (Fig. 5 and Table 1). Crosssties were not only placed in the concrete layer, but they also used in the void regions to provide a regular pattern of shear support as shown in Fig. 5. The clear cover is used as 15 mm.

2.2 Analytical modelling using finite element method

Finite element analysis methods are used in many different areas, such as in the modeling of sensitive materials, concrete and steel. Load, stress, displacement, temperature, etc. values are transferred from node to node and the type of the analysis method affects the results. Since many researchers modeled the reinforced concrete slabs using ABAQUS software which considers Explicit Dynamic Analysis (EDA) [18, 25, 29, 32], same software and technique was utilized in this study. There are some behavioral problems during the modeling process of reinforced concrete members such as dynamic effects, non-linear behavior, plastic deformations and contact uncertainty [45, 46]. Explicit Dynamic Analysis is a useful tool to overcome these problems as recommended in many studies. In addition, concrete damage plasticity (CDP) model for concrete, elastoplastic material models for steel, relevant support conditions, type of contact between contact surfaces and mesh sizes were the other issues to be determined during the modeling. Considering the several parameters

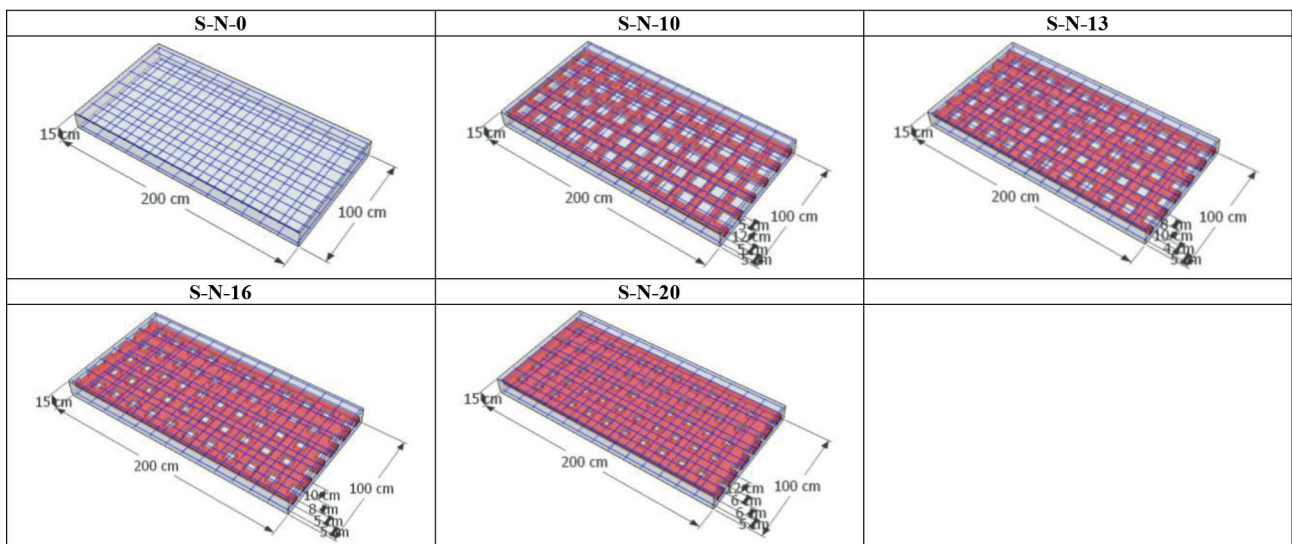


Fig. 1 Group S-N slabs

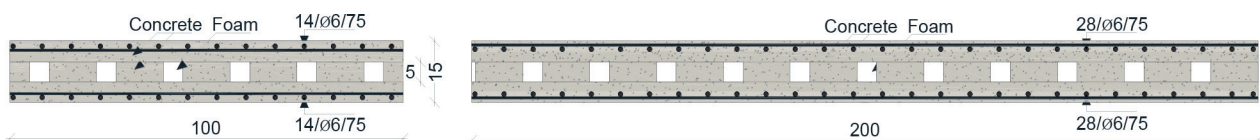


Fig. 2 Cross sections and reinforcement details of the slabs in Group S-N (distances in cm and rebar dimensions in mm)

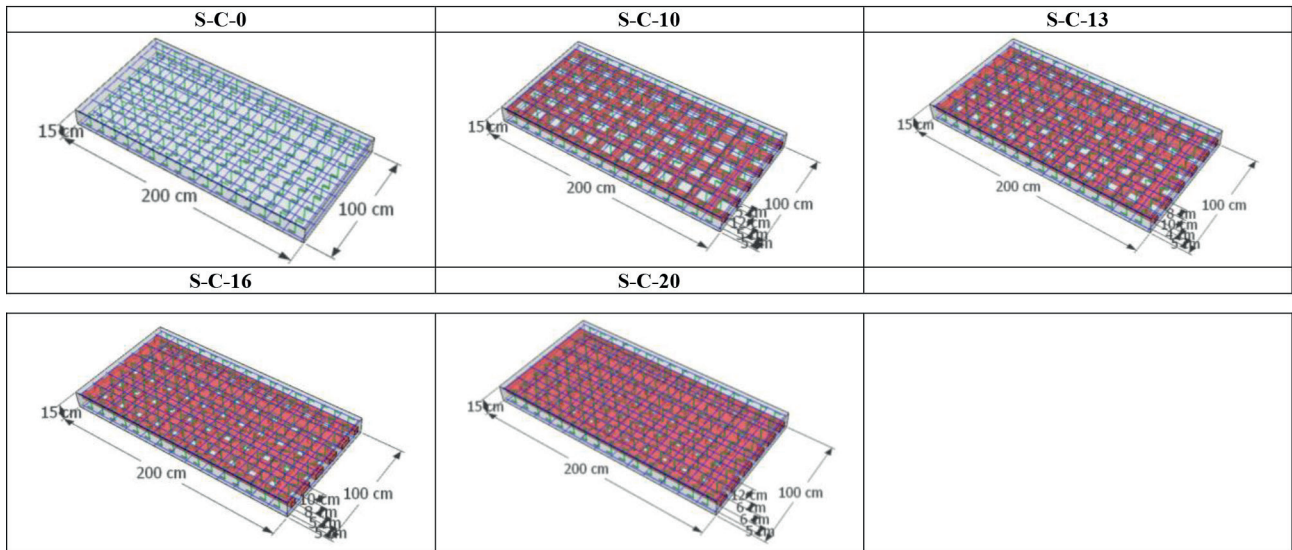


Fig. 3 Group S-C slabs

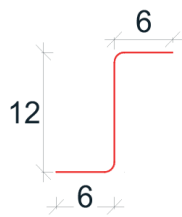


Fig. 4 Crosstie geometry (dimensions in cm)

mentioned above, it was stated that the results from the analytical models were compatible with the experimental results [18, 25, 29, 32].

In this study, upon the reliable results presented in the literature, ABAQUS software with Explicit Dynamic Analysis method was utilized in modeling the slabs and relevant material models, loading conditions and restraints was used. During the dynamic analysis, the loading is performed in very small steps to find the most reliable result [45, 46].

2.2.1 Boundary conditions and load procedure

All the slabs were 3D modeled in ABAQUS/Explicit software considering simply supports at both ends (short sides) to demonstrate the three-point-bending test. Slabs were loaded at the midspan by a line loading that was increased gradually until failure (Fig. 6). Moments, support reactions and midspan displacements were recorded continuously during the analysis.

Reference points (RP) RP-1, 2 and 3 were assigned to the semi-circular support surface center and connected with the center as a "tie". Linear tie (fixed in all directions) connection is assigned to the surface interaction between the supports and the slab. Supports are defined as master surface and slab is defined as slave surface. The load at the RP-1 point was defined as displacement and transferred to the slab as a linear load. The RP-2 point is fixed in all directions, while the RP-3 point is fixed in all directions except the x direction. For the displacement velocity, preliminary analyzes were made as 1, 3, 6, 7, 9 and 12 mm/s, and finally 6 mm/s was determined. Due to the low displacement velocity, the analysis was finished before the total collapse. When the displacement velocity was high, it was realized that impact was governed resulting in unreliable capacity. Support reactions and midspan displacements were recorded continuously during the analysis. Moments calculated by multiplying the support reactions by half span.

2.2.2 Finite element mesh size for slab and solution procedure

There are many mesh shapes (square, rectangular, triangular prism etc.) in finite element method. In order to accurately transfer stresses, strains and cracks, it is necessary to determine the appropriate mesh shape and size depending

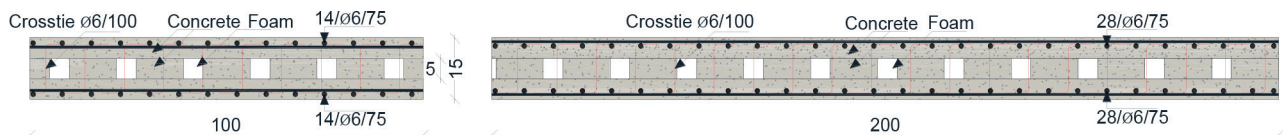


Fig. 5 Cross sections and reinforcement details of the slabs in Group S-C (distances in cm and rebar dimensions in mm)

Table 1 Slab properties

Slab	Concrete width at the mid-height layer between voids, cm	Void ratio %	Weight, kN	ρ	Crosstie Ratio in 1 m ² area
S-N-0	NA	0.0	7.50	0.0026	-
S-N-10	12	10.0	6.60	0.0026	-
Group S-N	S-N-13	10	6.19	0.0026	-
	S-N-16	8	5.85	0.0026	-
	S-N-20	6	5.59	0.0026	-
	S-C-0	NA	7.50	0.0026	0.0034
	S-C-10	12	6.60	0.0026	0.0034
Group S-C	S-C-13	10	6.19	0.0026	0.0034
	S-C-16	8	5.85	0.0026	0.0034
	S-C-20	6	5.59	0.0026	0.0034

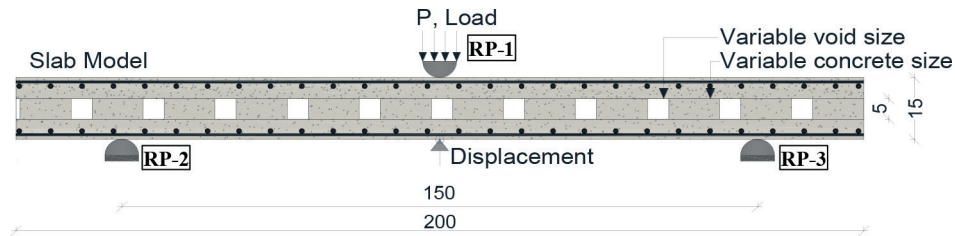
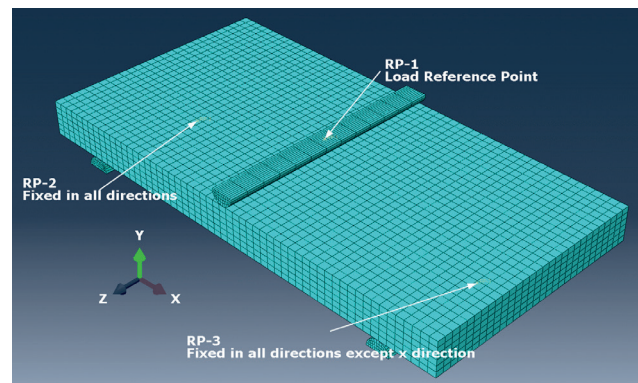
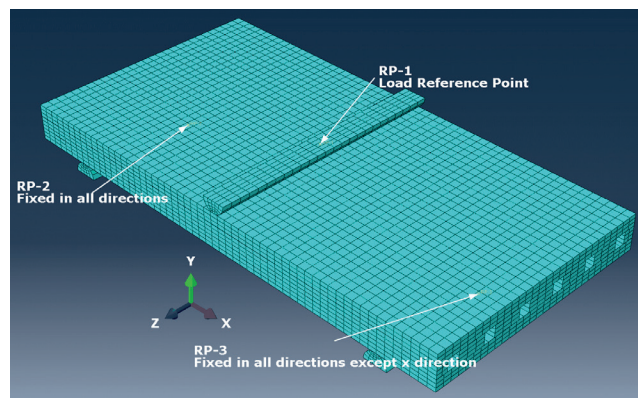


Fig. 6 Slab under three-point-bending test (distances in cm)

on the slab size. For the slabs, ABAQUS recommends the standard 8-node cube or rectangular prism mesh type [46, 47]. This type of FE provides smooth and correct load distribution. For this reason, preliminary analyzes of 20, 25, 30, 35, 40, 50 mm cube and rectangular mesh were performed for control slabs (S-N-0 and S-C-0) and from the analysis results it was decided to use a mesh size of 35 mm vertically and 25 mm horizontally (Fig. 7). For the remaining slabs, 35 mm vertical and 16.67 mm horizontal meshes were utilized. A smaller mesh was used horizontally to obtain more detailed and reliable tensile, and compression stresses. The reason for the difference in mesh sizes is to get rid of the convergence problem and save time during the analysis. While meshing, C3D8R mesh element type given in Explicit/3D Stress in ABAQUS was selected. As a result, 9918 elements and 12180 nodes were formed in S-N-0 slab, 12222 elements and 19152 nodes were formed in S-N-10 slab. Reinforcements in the short and long directions are defined as T3D2 material and the mesh size was 20 mm. Central-difference time integration rule, which eliminates the complex analysis, was followed [47]. Since EDA procedure proceeds using the small-time increment, time period 10 s was used in the analysis and geometric nonlinearity was taken into account. Increment type was taken automatically to shorten the analysis time. Other parameters were used as default as given in ABAQUS.



(a)



(b)

Fig. 7 Finite element meshes for slab (a) S-N-0, (b) S-N-10

2.2.3 Concrete model

The concrete damaged plasticity model (CDP) defined in [48] were used to define concrete properties in the ABAQUS software. In the CDP model, concrete stress-strain, damage parameter-inelastic strain graph and five plastic parameters are used. The first parameter is the dilatation angle of the concrete obtained from the Mohr Circle as shown in Fig. 8(a).

The dilatation angle (dilatancy, ψ) affects the stress and strain curve of the concrete. It can change not only the plastic deformation state, but also the fracture mode if it is too large or too small [49]. In the CDP model, the dilatation angle has a critical role in affecting the behavior among many parameters. In reinforced concrete studies where this model was used, the dilatation angle was generally investigated between 5° and 55° in order to accurately observe the experimental behavior of the elements [49–53]. For normal weight concrete, Wosatko et al. [49] did not recommend a value greater than 35° . Genikomsou and Polak [50] observed more accurate results when taking this value as 40° for concrete with a compressive strength of 33–46 MPa while analyzing punching behavior of the slabs. Guo et al. [51] suggested 38° for concrete with a compressive strength of 30–50 MPa, while Hafezolghorani et al. [52] suggested 31° . On the other hand, Rewers [53], used 35° in the reinforced concrete beam analysis for 39 MPa concrete. As can be seen, the dilatation angle value has been used to calibrate analytical model of a reinforced concrete element. In the preliminary analysis performed in this study, the results were evaluated by taking into account the dilatation angle of 30° , 33° , 35° , 38° and 40° . After interpreting the preliminary results, it was decided that to use 38° .

The second parameter is the eccentricity which is calculated from the intersection of the tangent line with the normal stress axis (Fig. 8(a)). Default value of the eccentricity is 0.1 in ABAQUS was recommended and used in many studies [47, 50, 51, 54, 55]. Therefore, an eccentricity value of 0.1 was utilized in this study. The third parameter is $F = f_{b0} / f_{c0}$ which is defined as the ratio of the yield strength of concrete under biaxial compression to the yield strength under uniaxial compression. Although its effect on the behavior is insignificant, the default value of 1.16 as recommended and used in many studies is considered in this study also. The fourth parameter is K_c which is the ratio of the second stress constant on the tension meridian to the stress constant on the pressure meridian. It is also defined as the shape of the yield surface in the

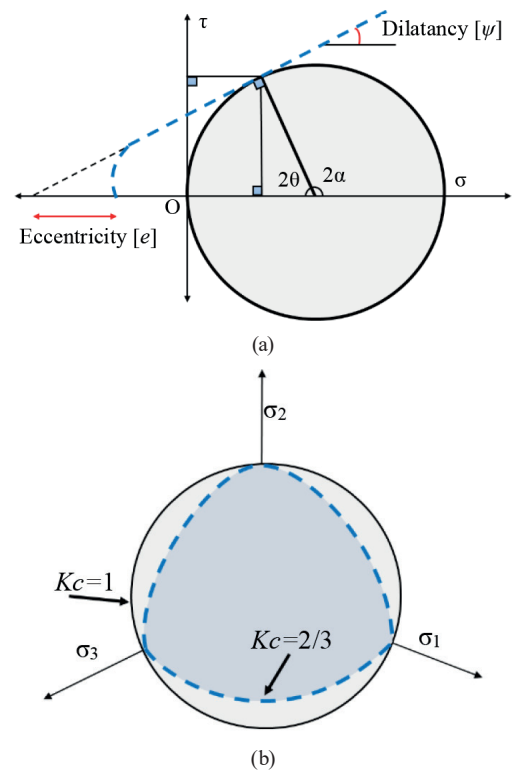


Fig. 8 (a) Eccentricity and dilatation angle (b) $K_c = 1$ and $K_c = 2/3$ parameters

strain plane [47]. In the Drucker-Prager concrete model, K_c value is usually taken as $2/3$ which is also the default value CDP model in ABAQUS (Fig. 8(b)).

The fifth parameter is the viscosity (μ). This is a parameter representing the resolution time of the developed viscoplastic system of the CDP model [47]. It is a parameter that affects the convergence problems, analysis time, number of iterations, stiffness, load carrying capacity, stress and strain values in the analysis process. Viscosity is used to save time without disturbing the results. It also helps to improve the convergence ratio [56]. Higher value reduces the analysis time significantly, but the results diverge from the actual behavior.

Therefore, a value greater than 0.0005 is not recommended [56]. For beams and slabs, 0.1×10^{-4} or 1×10^{-5} was taken mostly [50–54]. In this study, viscosity was assumed to be "0" (zero) to avoid convergence problem and to find more consistent results. The five parameters given above to define the concrete properties are based on the literature as given in Table 2.

In this study, the concrete model defined in the Chinese Code-2010 [57] was used to obtain the stress-strain values of C30/37 concrete. Stress-strain and damage parameter-inelastic strain curves of concrete under uniaxial compression and tension are depicted in Table 3. Nonlinear

Table 2 Concrete plastic damage model parameters

C30/37 Concrete		References
f_c [MPa]	30	
f_{ct} [MPa]	1.917	[44] ($f_{ct} = 0.35\sqrt{f_c}$)
Density [t/m ³]	2.5	[58]
Elastic Properties		
E_c [MPa]	27386	[59] ($E = 5000\sqrt{f_{ck}}$)
Poisson's ratio [ν]	0.2	[44, 60]
Plastic Properties		
Dilation angle, [ψ]	38°	[51]
Eccentricity [e]	0.1	[47, 50, 51, 54, 55]
$F = f_{b0}/f_{c0}$	1.16	[47, 50, 51, 54, 55]
$K_c = q'_{CM}/q'_{CM}$	2/3	[47, 50, 51, 54, 55]
Viscosity [μ]	0	[50, 51, 54]

parabolic relationship is used for compression behavior. The yield point under compression was calculated as 40% of the maximum strength (f_c) ending up 12 MPa. Compressive stress decreases parabolically after f_c until 3.05 MPa. However, as for tensile behavior it is assumed that a linear relationship exists between stress and strain up to maximum tensile stress (f_{ct}) and an abrupt decrease in stress exists after the f_{ct} . Compressive stress-strain and tensile stress-strain curves according to the Chinese Code-2010 [57] are given in Fig. 9.

Table 3 Stress-strain and damage parameter- inelastic strain curves of concrete under uniaxial compression and tension

Compression	Tension
$\sigma_c = (1 - d_c) E_c \varepsilon$	$\sigma_t = (1 - d_t) E_c \varepsilon$
$d_c = \begin{cases} 1 - \frac{n\rho_c}{n-1+x^n} & x \leq 1 \\ 1 - \frac{\rho_c}{a_c(x-1)^2+x} & x > 1 \end{cases}$	$d_t = \begin{cases} 1 - \rho_t [1.2 - 0.2x^5] & x \leq 1 \\ 1 - \frac{\rho_t}{a_t(x-1)^{1.7}+x} & x > 1 \end{cases}$
$\rho_c = \frac{f_{cu}}{E_c \varepsilon_{cu}}$	$\rho_t = \frac{f_{tu}}{E_c \varepsilon_{tu}}$
$n = \frac{E_c \varepsilon_{cu}}{E_c \varepsilon_{cu} - f_{cu}}$	

In $x = \varepsilon/\varepsilon_{cu}$, the sub-index c and t represent pressure and tension, respectively. E_c is the modulus of elasticity, $\sigma_{c,t}$ is the calculated stress, $d_{c,t}$ is the damage parameter, ε is the strain parameter, $f_{cu,tu}$ is the ultimate strength, $\varepsilon_{cu,tu}$ is the peak strain. For the ultimate stress in C30/37 concrete a_c value is 1.36, for the ultimate tensile stress of 1.917 MPa a_t value is 1.16 found iteratively.

Elastic region of the concrete under compression and tension is defined introducing the modulus of elasticity and Poisson's ratio values given in Table 2 [44, 47, 50, 51, 54, 55, 58-60], while the plastic region is defined using the

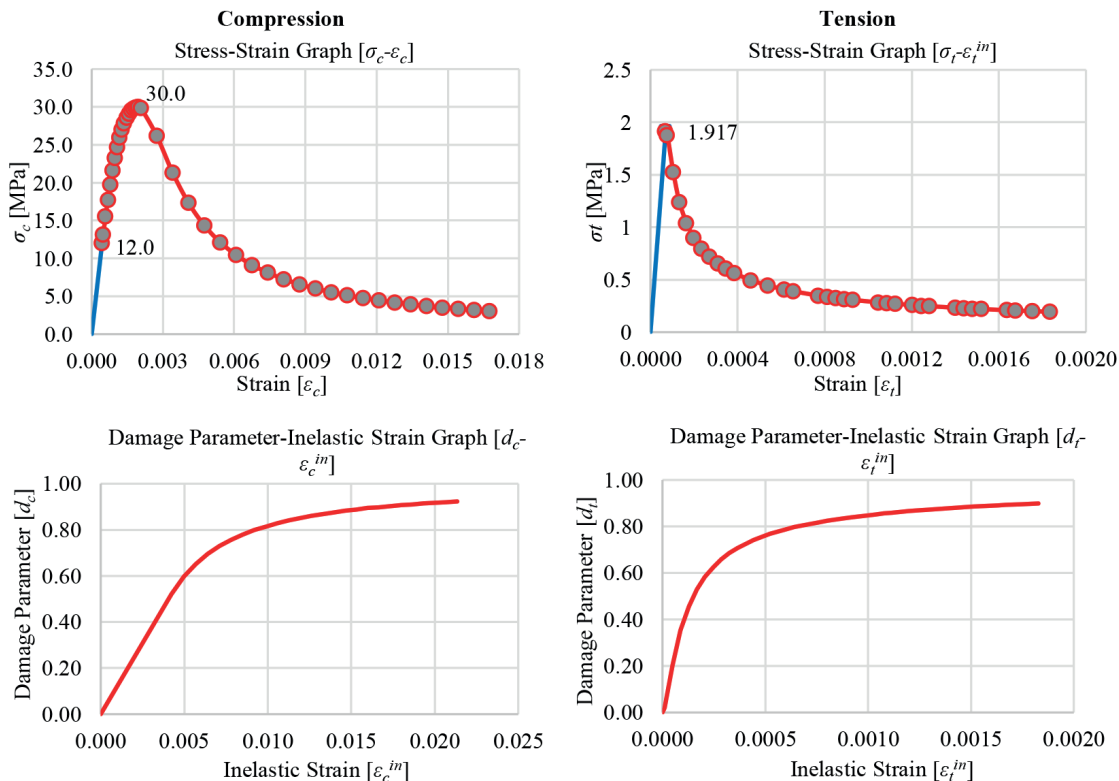


Fig. 9 C30/37 concrete material models in compression and tension

concrete damaged plasticity model in ABAQUS. Thus, the dotted curves in Fig. 9 were defined as the concrete damaged plasticity model. Since concrete is damaged after the yield strength, change in the strength and stiffness in cyclic loading can be measured to identify the damage. In this study, concrete damage percentage and inelastic strain values are also defined, and the curves related to these values are presented in Fig. 9. The damage increased with the deformation under compression and large deformations occurred after approximately 60% damage (d_c). Between 80% and 90% damage rate, much higher inelastic strains develop. The amount of inelastic strain increases rapidly after 70% damage (d_t) under tensile stress.

Considering the stress-strain curve of the concrete, d_c compression damage parameter, ε_t^{el} elastic strains and ε_t^{in} inelastic strains were calculated from Eqs. (1), (2) and (3), respectively. As for tension parameter ε_t^{el} and ε_t^{in} of concrete, the same equations were utilized. According to the concrete data in the equations f_c compressive strength, ε_c uniaxial strain under compression, ε_{0c}^{el} elastic strain, ε_c^{in} inelastic strain, ε_t tensile strain, ε_t^{el} elastic tension strain and ε_t^{in} inelastic tensile strain of concrete are determined by the following equations [47]:

$$d_c = 1 - \frac{f_c}{f_{cu}}; \quad d_t = 1 - \frac{f_t}{f_{cu}}, \quad (1)$$

$$\varepsilon_{0c}^{el} = \frac{f_c}{E_0}; \quad \varepsilon_{0t}^{el} = \frac{f_t}{E_0}, \quad (2)$$

$$\varepsilon_c^{in} = \varepsilon_c - \varepsilon_{0c}^{el}; \quad \varepsilon_t^{in} = \varepsilon_t - \varepsilon_{0t}^{el}. \quad (3)$$

The plastic parameters are calculated according to the following equations, taking into account the compressive and tensile strength and inelastic parameters of the concrete defined in the ABAQUS software. Plastic strain in compression ε_c^{pl} , plastic strain in tension ε_t^{pl} are given as in Eq. (4) [47].

$$\varepsilon_c^{pl} = \varepsilon_c^{in} - \frac{d_c}{1-d_c} \frac{f_c}{E_c}; \quad \varepsilon_t^{pl} = \varepsilon_t^{in} - \frac{d_t}{1-d_t} \frac{f_t}{E_c} \quad (4)$$

2.2.4 Rebar model

In order to simplify the calculations, the stress-strain curve of the rebar under tension was formed from three linear lines idealized with the values taken from TEC-2018 [61]. Elastic and plastic parameters were calculated and given in Table 4 [30, 50, 53, 54, 58, 60-62]. B420C rebar was assumed with a yield strength (f_{sy}) of 420 MPa and tensile strength (f_{su}) of 525 MPa. The amount of stress-inelastic

Table 4 Mechanical properties of B420C rebar

B420C Steel		References
f_{sy} [MPa]	420	[61]
f_{su} [MPa]	525	[61] ($f_{su}/f_{sy} = 1.25$)
Density [t/m ³]	7.85	[58, 60, 62]
Elastic Properties		
E_s [GPa]	200	[61]
Poisson's ratio[v]	0.3	[30, 50, 53, 54]
Plastic Properties		
Stress [MPa]	ε_t^{in}	
420	0	[61]
420	0.0059	
525	0.0779	

strain (ε_t^{in}) in the plastic region of the reinforcement was calculated by subtracting the elastic strain at the point where it reached the yield strength from all strains.

3 Results and discussion

As previously noted, voided slabs were created by using polystyrene foam between two slab layers. Slabs were 3D modeled using ABAQUS and they were analyzed under distributed line load applied at the midspan. The aim was to understand the effect of voids on flexural behavior of slabs and also the effect of the crossties as it has been observed that vertical crossties increase the moment and shear capacities [35, 39, 42, 43].

3.1 Tensile damage ratio and plastic strain distribution

Slabs were examined under the gradual line load up to the failure. Fig. 10 and Fig. 11 shows the global tension damage ratio (DAMAGET) at the yield moment. Stripping the compression fiber only the tension region becomes visible as presented in Fig. 12. Only the concrete part is seen in Fig. 12 since polystyrene foams at the middle of the section were not modeled since they create voids and do not have any effect on the behavior.

It can be seen from Fig. 10 and Fig. 12 that; cracks were not localized at a region instead it spread to a large area indicating that the bottom of S-N-0 cracks completely. A_{cr} (in %) was calculated to represent the slab cracked areas. Therefore, $A_{cr,S-N}$ represents group S-N, $A_{cr,S-C}$ represents group S-C. The cracked area (A_{cr}) is almost 98% of the entire span. Group S-N slabs experienced significant cracks developed and localized below the voids. Those limited cracks barely penetrated to the top layers. Limited cracks developed which extended through the slab width.

As for S-C-0 it is seen that the same crack pattern as S-N-0 was possible and additional cracks developed resulting in a cracked region of 100% of the span. Introducing voids again narrowed the cracked regions and decreased the moment capacity (Figs. 10, 11 and Table 5). However, decrease in A_{cr} and M_y was less than Group S-N slabs which can be attributed to the effect of crossties. Since crossties connect the tension zone with the compression zone, they did not allow both zones to behave separately. While a tension zone at a region was cracked, owing to the crossties, the force could be redistributed to the adjacent regions which resulted in a greater cracked region when compared

to Group S-N slabs. Therefore, redistribution of stresses was said to be more pronounced in voided slabs having crossties. Higher cracked region ended up higher moment capacities and higher load carrying capacities. Yield moment capacity (M_y) reduced 7% with the introduction of 10% void ratio (S-C-10) and it further decreased 45% with 20% void ratio (S-C-20). Those reductions in M_y were less than the slabs without crossties. Besides, it can be seen from Fig. 12 and Fig. 13 that 10% void ratio (S-C-10) decreased the cracked region 19% (less than the one in S-N-10 which was 30%) and 20% void ratio (S-C-20) reduced the cracked region 62% (reduction was 76% in S-N-20).

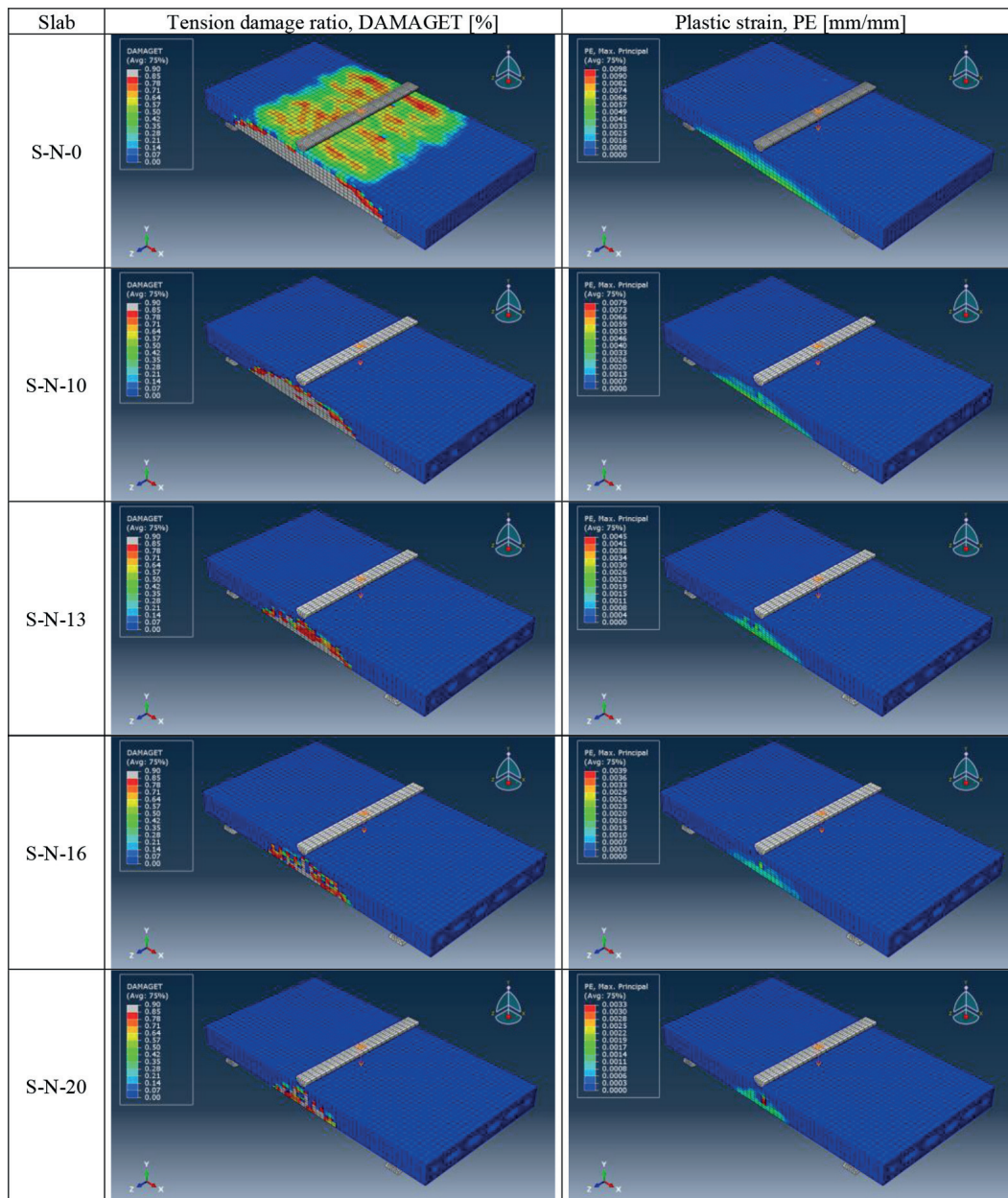


Fig. 10 Tensile damage ratio and plastic strain distribution of S-N slabs

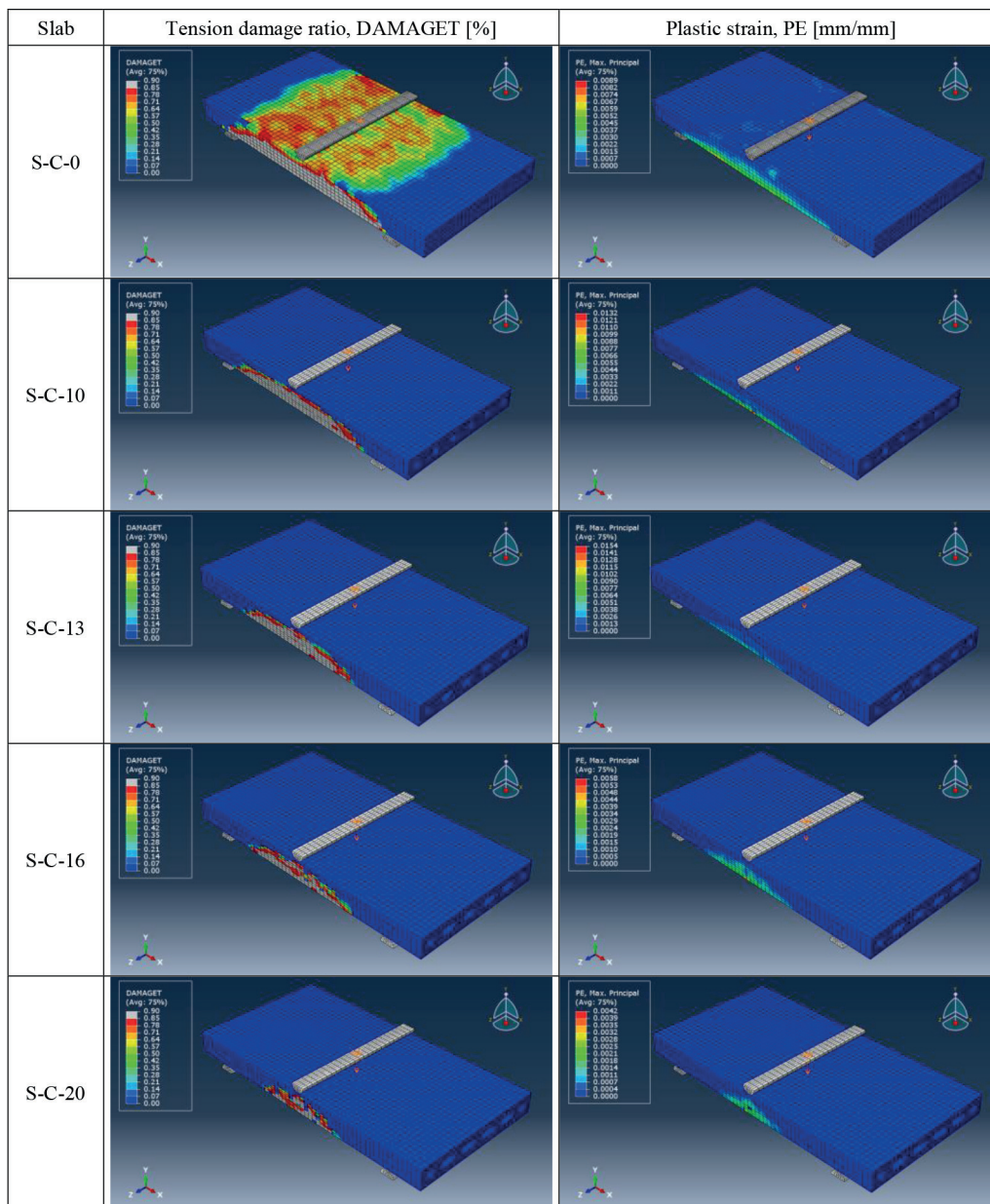


Fig. 11 Tensile damage ratio and plastic strain distribution of Group S-C slabs

Comparing both slab groups, it can be said that introducing cross-ties enhances the behavior of slabs and widens the cracked region. The effects of cross-ties are more pronounced in slabs having higher void ratio. Comparing S-N-10 with S-C-10 it is seen that 15.71% increase in A_{cr} is possible in the slabs having a 10% void ratio. Noticeable increase is observed in S-C-20 where A_{cr} increased 58.33% when compared to S-N-20.

3.2 Equivalent stress distribution

Von Mises equivalent stress distribution for the slabs were presented in Fig. 14. It can be seen that although equivalent stresses distributed over the solid slab in S-N, it started

to be narrow with the introduction of the voids. As voids increased, much narrower stress distribution was seen.

When cross-ties were used in the slabs (Group S-C slabs), a larger area of highly stressed region was possible as seen from Fig. 14. The large of highly stressed region ended up more cracks and crushing thus resulting in greater moment capacities.

3.3 Flexural behavior of S-N slabs

Bending moments (shortly moments) at each load level were calculated from the reaction forces taken from the supports and vertical displacements at each load level were recorded directly from the lower part in the middle

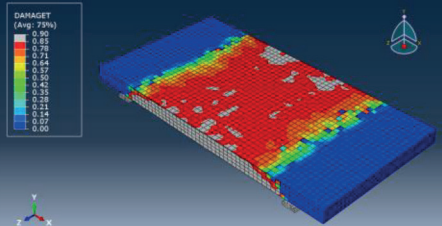
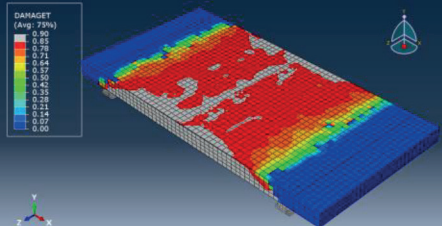
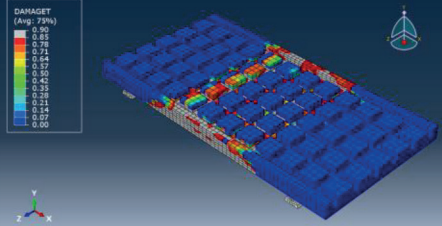
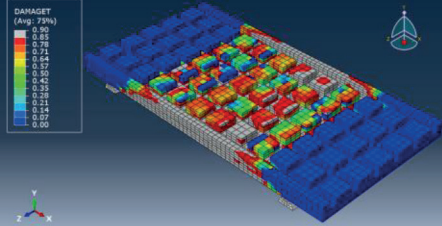
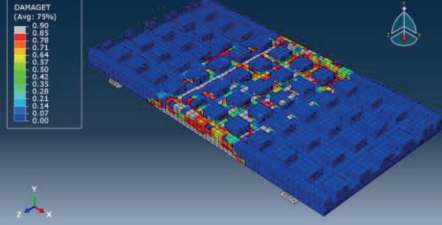
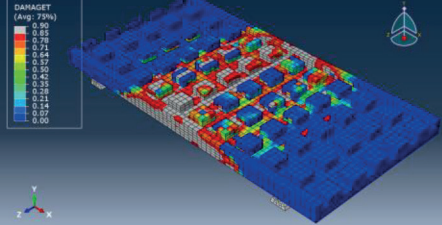
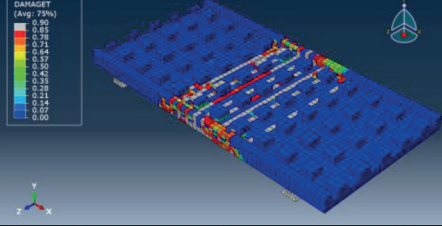
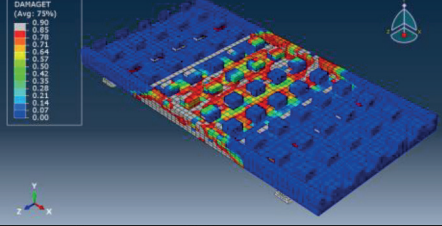
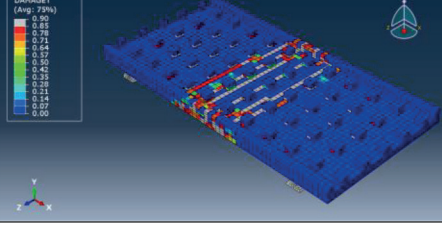
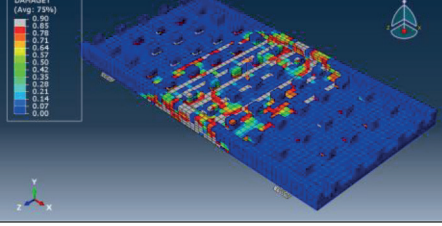
Slab	Tensile damage ratio in the middle of the slab section, DAMAGET [%]	$A_{cr,S-N}$ %	Slab	Tensile damage ratio in the middle of the slab section, DAMAGET [%]	$A_{cr,S-C}$ %	$A_{cr,S-C}/A_{cr,S-N}$ %
S-N-0		98	S-C-0		100	2.04
S-N-10		70	S-C-10		81	15.71
S-N-13		48	S-C-13		64	33.33
S-N-16		28	S-C-16		44	57.14
S-N-20		24	S-C-20		38	58.33

Fig. 12 Tensile damage ratio in the tension region

of the section. Moment capacity of the slabs was presented in Fig. 15 in terms of moment-vertical displacement.

Since slabs were tested under 3-point bending test setup and behaved like a beam, Eq. (5) can be used to calculate the moment capacity of the solid slab (M_r) ignoring compression reinforcement. In the equation A_s stands for the tensile reinforcement (which is $14\phi6$), f_y is the yield strength of the rebar (420 MPa) and jd is the moment arm where d is the effective depth of the slab (135 mm). jd is mainly given by Eq. (6) and for doubly reinforced flexural members j varies between 0.86-0.90. In Eq. (6). k_1 is the modification factor for the neutral axis (c). Ersoy et al. [63]

Table 5 Yield moment (M_y) capacities $M_{y,relative}$

Slab	M_y , kNm	$M_{y,relative}$	Slab	M_y , kNm	$M_{y,relative}$
S-N-0	19.0	1.00	S-C-0	21.5	1.00
S-N-10	13.0	0.68	S-C-10	20.0	0.93
S-N-13	11.5	0.61	S-C-13	15.0	0.70
S-N-16	10.7	0.56	S-C-16	13.0	0.60
S-N-20	10.0	0.53	S-C-20	11.8	0.55

recommended 0.86 for j and using this value M_r was calculated as 19.3 kNm which can be considered as the yield moment capacity because of the yield strength of the rebar. As it is seen from Fig. 15, moment capacity of the solid

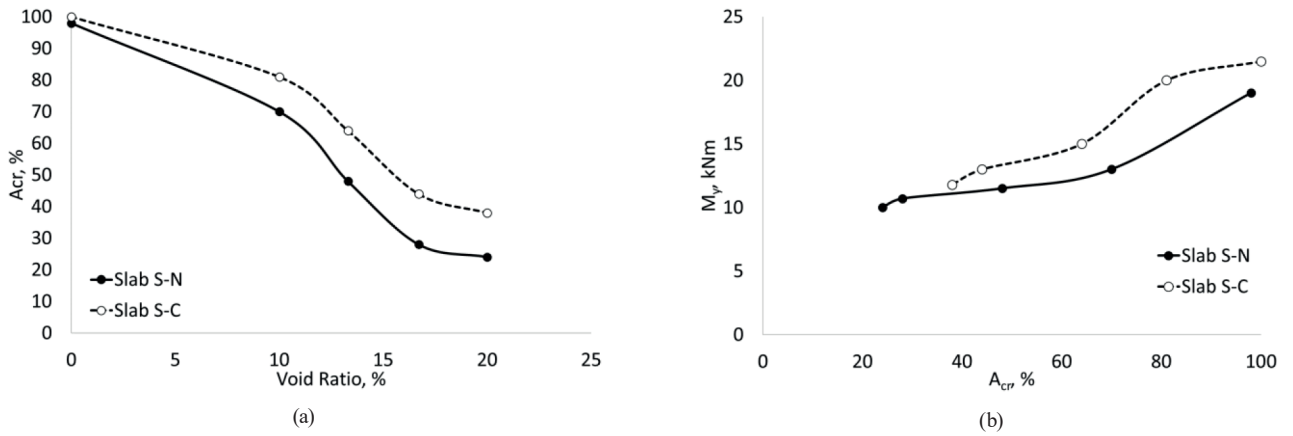


Fig. 13 Comparison of A_{cr} and M_y wrt. void ratio (a) A_{cr} vs Void Ratio, (b) M_y vs A_{cr}

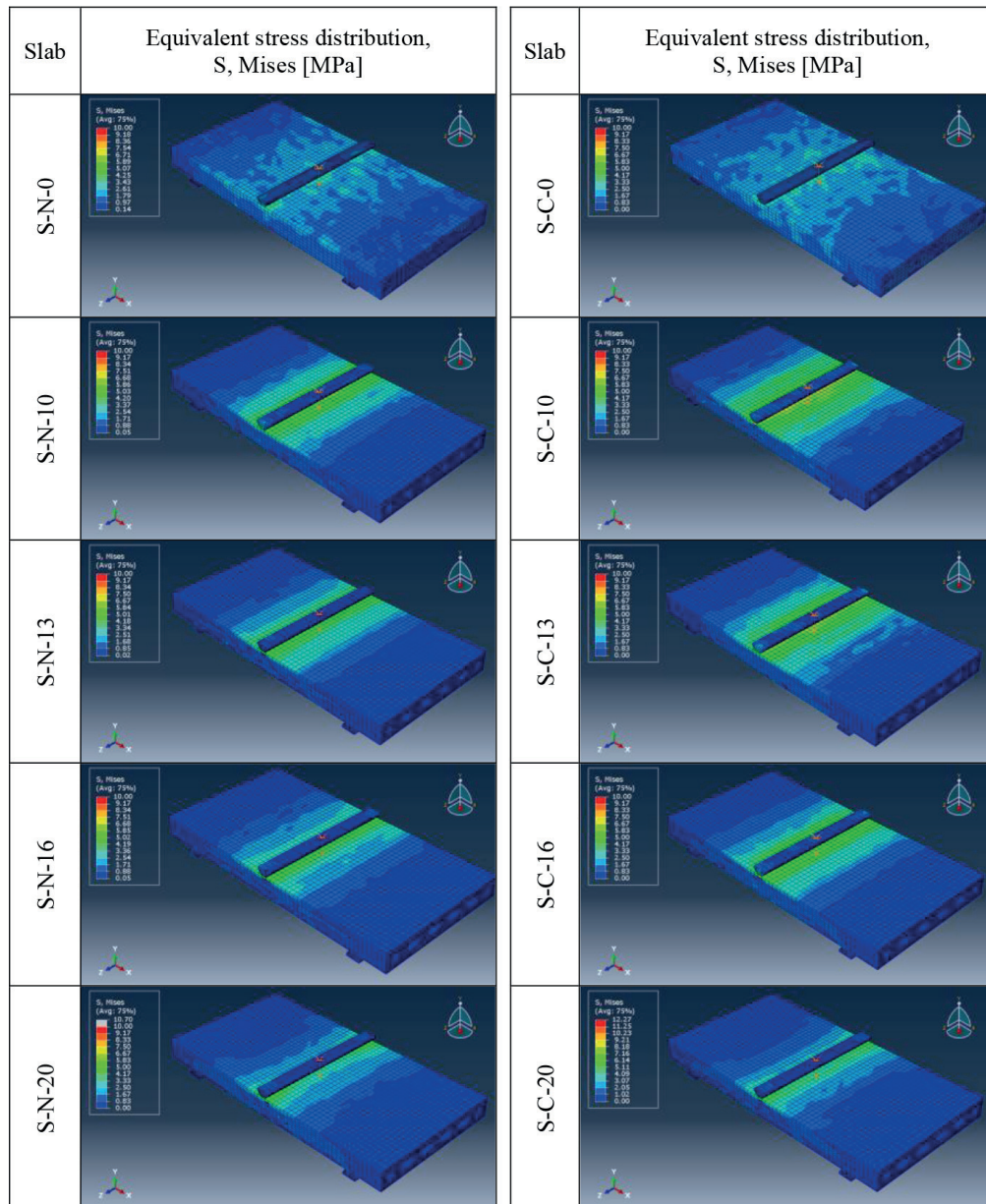


Fig. 14 Equivalent stress distribution

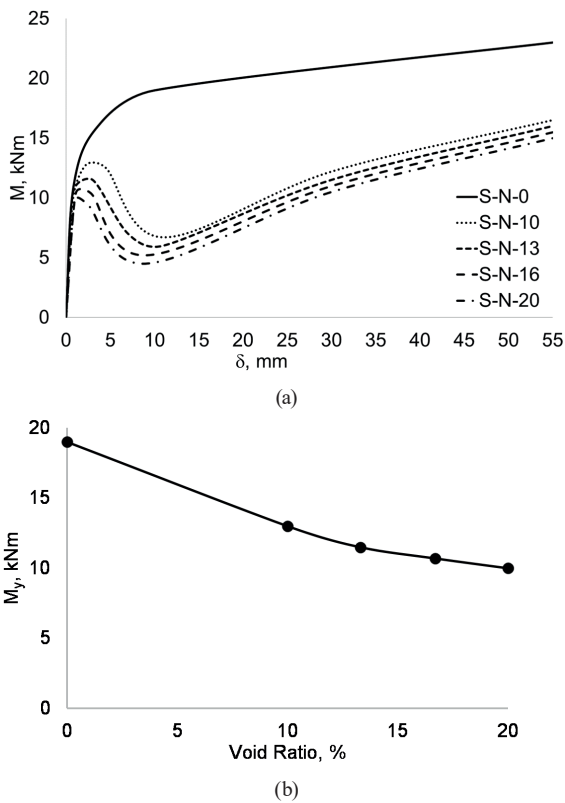


Fig. 15 Moment-displacement curves of S-N slabs (a) Moment-displacement curves, (b) M_y vs void ratio

slab of S-N-0 had a yield moment capacity of 19 kNm which is close to the hand calculation. Eq. (5) was used as a calibration tool for the analytical model and getting close capacities it was assumed that the model was quite representative and reliable therefore the same modeling technique was used to model the rest of the slabs.

$$M_r = A_s f_y j d \tag{5}$$

$$j d = \left(d - \frac{k_1 c}{2} \right) \tag{6}$$

Increase in the void ratio resulted in reduced cracked region and reduced moment capacity as shown in Fig. 15(b) 10% void ratio reduced the cracked region 30% and thus reduced yielding moment capacity (M_y) by 32%. When the void ratio increased to 20%, the cracked area narrowed to 24% of the slab and M_y decreased 47% as shown in Table 5.

Solid slab reaches M_y with a high stiffness and after that post-yield stiffness significantly reduced but moment capacity slightly and continuously increased up to M_u (23 kNm). The curve was similar to the moment-curvature curve of a typical ductile beam. However, behavior of the voided slabs differed too much. They had a sharp decrease upon yielding (Fig. 15(a)) which can be attributed to the

reduced compression region due to the voids. It is known that neutral axis depth is great at low strain values and starts to decrease upon the increase in strain of tension rebar. Increase in the strain of tension rebars resulted in decrease in neutral axis depth. Reducing neutral axis depth increased the moment arm and thus increased the moment capacity again. Besides, post-yield moment increase for voided slabs was well pronounced due to the strain hardening of the rebar as compared to the solid slab.

3.4 Flexural behavior of S-C slabs

As previously mentioned, S-C slabs had cross-ties creating direct connections between tension and compression fibers of the concrete. Although axial tension and compression forces develop in the slab (in most of the flexural members) and balance each other, force distribution is possible via shear transfer. As the voids reduce the shear area at the highly stressed midheight of the slab, force transfer becomes harder and results in a sharp decrease upon yielding. Cross-ties extending from top to the bottom of the slab will carry the shear and enable force transfer and contribute to the ductile bending of the slab.

Fig. 16 shows the flexural behavior of S-C slabs. It can be seen from Fig. 16(a) that the solid slab again experienced a smooth behavior, that is no significant change was

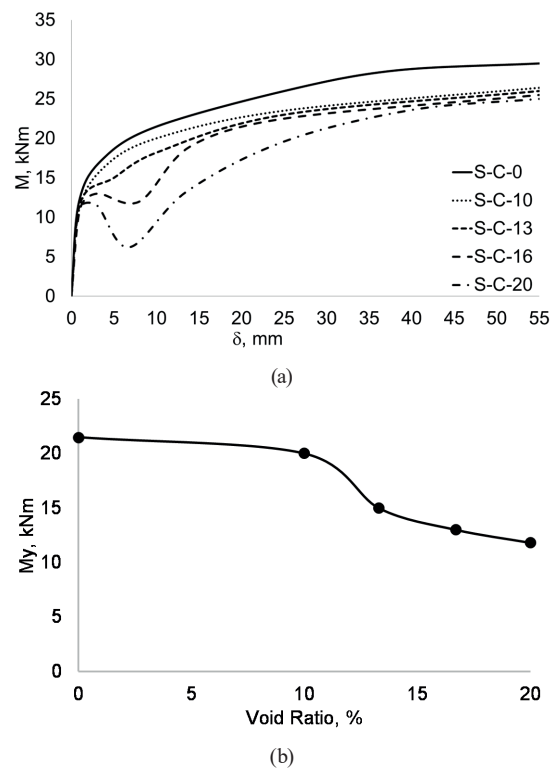


Fig. 16 Moment-displacement curves of S-C slabs (a) Moment-displacement curves, (b) M_y vs void ratio

seen in the curve. As in ductile flexural members, stiffness reduced significantly beyond the yielding and member failed at M_u . Although all the voided slabs had sharp decrease in moment capacity beyond M_y in S-N slabs, introducing crossties altered this behavior. Since crossties enabled the shear transfer between tension and compression regions smooth flexural behavior was obtained for 10% void ratio in S-C-10. In other words, 10% void ratio with crossties seem not to affect the flexural behavior. When void ratio increased to 13.3% (S-C-13.3) almost zero stiffness region was observed after M_y and with strain hardening moment capacity started to increase afterwards. With 16% void ratio (S-C-16), effect of crossties reduced and slight decrease in moment capacity was seen beyond M_y . This reduction however easily recovered with both the reduction in neutral axis depth and strain hardening of

rebar. Significant decrease was observed in the slab having 20% void ratio (S-C-20) beyond M_y indicating that the amount of crossties were not adequate to transfer the shear.

Change in yield moment capacity with void ratio was given in Fig. 16(b) It is seen that crossties were quite effective in voided slabs. No significant reduction was seen in 10% void ratio. Although decrease was well pronounced in higher void ratio, general behavior was not affected in 13.3% void ratio as well. It can be said that amount of crossties was not adequate when void ratio increased beyond 13.3%.

3.5 Comparison of the flexural behavior

Fig. 17 gives the Moment-displacement (M-d) behavior of the slabs comparatively. As it is seen from Fig. 17(a), solid slabs behaved almost equally until M_y and beyond

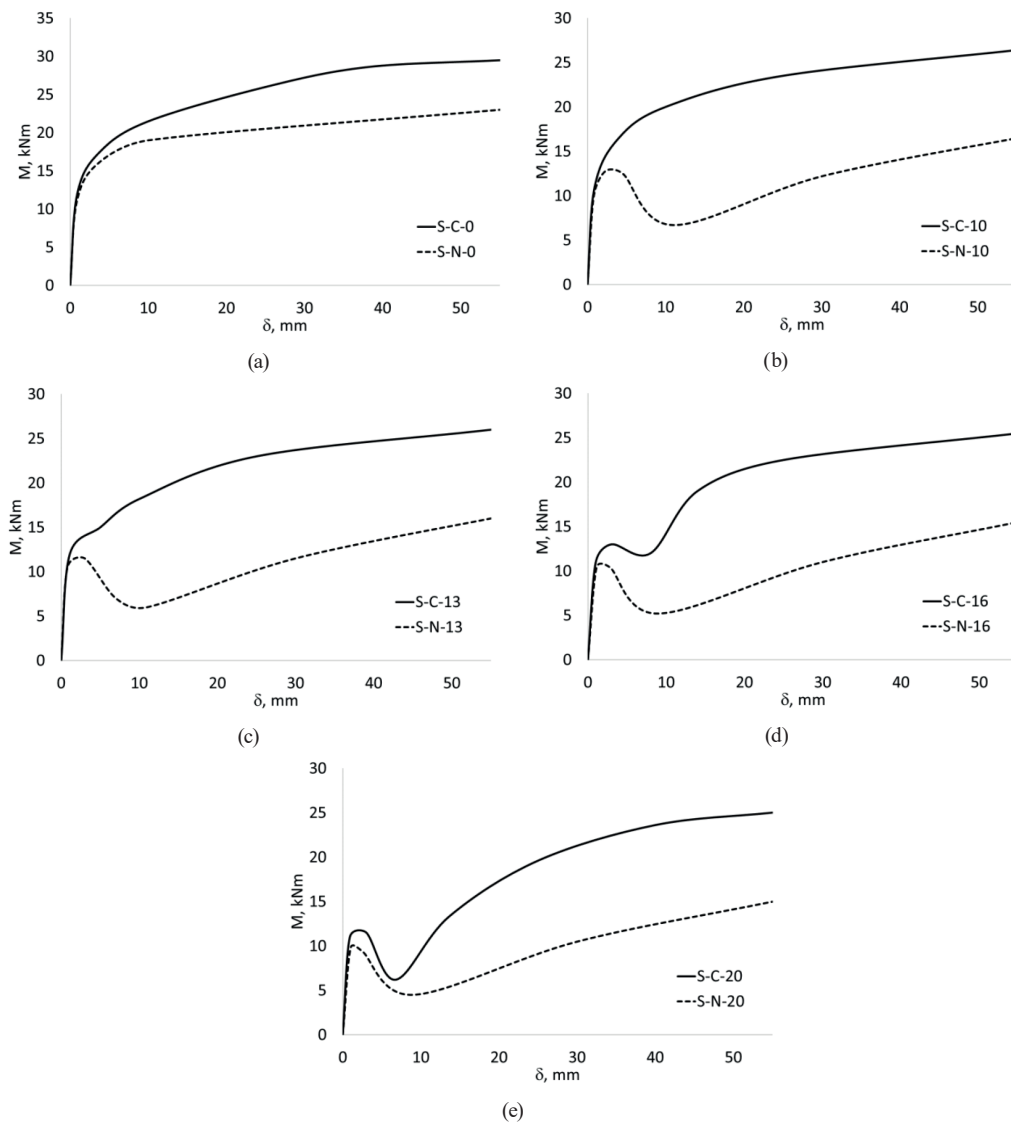


Fig. 17 Comparison of the M-d behaviors (a) M-d behavior of S-C-0 and S-N-0, (b) M-d behavior of S-C-10 and S-N-10, (c) M-d behavior of S-C-13 and S-N-13, (d) M-d behavior of S-C-16 and S-N-16, (e) M-d behavior of S-C-20 and S-N-20

M_y stiffness was almost zero in S-N-0 but S-C-0 still had increased moment capacity which can be attributed to the presence of crossties. Dramatic change was observed in slabs with a 10% void ratio. Although no decrease after M_y was seen in S-C-10, moment capacity reduced significantly (almost 50% reduction was seen) in S-N-10 which reveals the importance of crossties. As previously noted since crossties connect tension fibers to the compression ones shear transfer was possible and relatively more ductile behavior could be attained. Similar behavior was visible in Fig. 17(c) in slabs with 13.3% void ratio. Although reduction in moment capacity after M_y was seen in slabs having 16.7% and 20% void ratio, it can be said that crossties are well effective in S-C-16 and S-C-20 slabs. Therefore, it can be said that voids reduce the moment capacity and energy dissipation capacity, however crossties may alter this behavior if adequately used in the slabs. From the analysis performed in this study it was seen that 0.34% crossties were adequate in slabs having void ratio less than 16.7%.

3.6 Recommended moment capacity

There is limited research concerning the moment capacity of voided slabs. Marais [64] stated that except for the self-weight and bending stiffness of the slab, flexural behavior of the voided (spherical voids) slabs were almost the same as the solid slabs. Subramanian et al. [65] recommended an equation to calculate the ultimate moment capacity for the spherically voided slabs and the only parameter taking the void into account was implemented in the neutral axis depth. They assumed that neutral axis depth was limited to the clear concrete above the voids. Al-Gasham et al. [23] after testing voided slabs, calculated the flexural strengths using ACI318-19 [66] and Eurocode 2 [60] and found that compression depth slightly penetrated into the voids and in general neutral axis depth remains in the solid part of the concrete above voids. In addition, compression reinforcement was stated to have an insignificant effect on the moment capacity. Therefore, although it is given for the solid members, ACI318-19 [66] and Eurocode 2 [60] was stated to be utilized to calculate the moment capacity of the voided slabs [23, 32]. Contrarily, Lee et al. [67] indicated that cracking moment predictions made in ACI318-19 [66] were nonconservative for voided slabs.

None of the studies proposed an equation considering the effects of voids on moment capacity. Researchers did not implement the effect of crossties (or any shear link members) on moment capacity calculations either.

In general design calculations, moment capacity of a beam or a slab is mainly considered to be equal to its yield capacity since less increase beyond M_y is noted (strain hardening is mainly ignored). Therefore, moment capacity (M_r) is generally calculated from Eq. (5) where j is the moment arm and it usually changes between 0.86 and 1.0. In this study compression reinforcements were ignored since their contribution to the moment capacity is insignificant. In Eq. (5) A_s, f_y and d are all constant for a typical slab. The only variable is j . It affects the moment capacity directly and the effect of voids and crossties should be implemented into j . Eq. (7) is proposed for the moment arm (j) in which v is the void ratio in %, and ρ_c is the crossties ratio in %.

$$j = 0.86 - \sqrt{\frac{v}{100}} + \left(\frac{\rho_c}{10}\right)^{0.7} \quad (7)$$

Fig. 18 shows the comparative results of the moment capacities. The dotted and dashed lines represent the analytical results from the 3D-modeling of the slabs. The solid back lines indicate the moment capacities calculated from Eq. (5). As it can be seen, taking void ratio and ratio of the crossties into account, moment capacities may be predicted with minor errors. The proposed equation is also conservative. Since the equations proposed by Subramanian et al. [65] and the one given in ACI318-19 [66] do not consider the void ratio and crossties; they assume a constant moment capacity which becomes nonconservative with the introduction of the voids. Therefore, from the results given in this article it is recommended to consider the voids and crossties to calculate the moment capacities of voided slabs.

4 Conclusions

In this study, the effect of cuboid voids on flexural behavior of slabs was investigated via 3D analysis using ABAQUS.

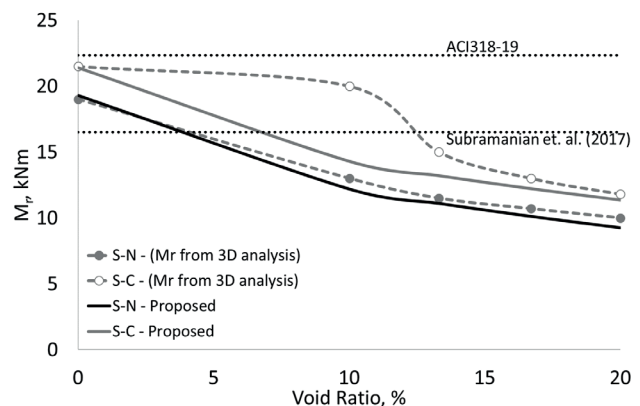


Fig. 18 Moment capacity prediction results

Two slab types were prepared: the first type had only voids, the second type had voids and crossties. From the analysis results following conclusions were drawn:

- Voids in the slab reduce the yield moment capacity of the slabs. Since the neutral axis depth is large at low load levels, the compression zone of the slab reduces owing to the voids and leads to a reduced moment capacity.
- The reduction in moment capacity can also be attributed to the reduced shear area which is responsible for the force transfer between tension and compression zones.
- Crossties have a significant effect on the behavior. They can be used to compensate the reduced shear transfer. They can also increase the moment capacity and ductility and thus improve the flexural behavior considerably.
- Voids reducing the shear area, also narrowed the cracking zone. Damage localized in a limited area and adversely affected the flexural behavior. However,

using crossties loss in shear was recovered and damage distributed in a large area resulting in improved and ductile flexural behavior.

- Neither codes nor researchers consider the void ratio and effect of crossties while calculating the moment capacity of a slab. Results in this study indicate that those parameters are important and should be taken into account. Therefore, a simple equation for the moment capacity of voided slabs with/without crossties was proposed. Results were reliable and conservative when compared to the equations available in the literature.

Acknowledgements

This study has been supported by Van Yuzuncu Yil University Scientific Research Projects Coordination Unit under grant number FDK10020. In addition, the library of Dicle University was used. It was studied within the scope of the first author's PhD thesis.

References

- [1] Pawar, A. J., Mathew, N. S., Dhake, P. D., Patil, Y. D. "Flexural behavior of Two-Way voided slab", *Materials Today: Proceedings*, 65(2), pp. 1534–1545, 2022.
<https://doi.org/10.1016/j.matpr.2022.04.500>
- [2] Yardim, Y. "Development of lightweight composite slab system for residential building", PhD Thesis, University Putra Malaysia, 2008.
- [3] Yee, A. A. "Structural and economic benefits of precast/prestressed concrete construction", *PCI Journal*, 46(4), pp. 34–42, 2001.
<https://doi.org/10.15554/pcij.07012001.34.42>
- [4] Bakis, A., Isik, E., El, A. A., Ülker, M. "Mechanical properties of reactive powder concretes produced using pumice powder", *Journal of Wuhan University of Technology*, 34(2), pp. 353–360, 2019.
<https://doi.org/10.1007/s11595-019-2059-1>
- [5] Boyd, J. W. "Haydite, expanded perlite and pumice as aggregates in lightweight concrete", MSc Thesis, University of Wyoming, 1949.
- [6] Tapan, M., Depci, T., Özvan, A., Efe T. Oyan, V. "Effect of physical, chemical and electro-kinetic properties of pumice on strength development of pumice blended cements", *Materials and Structures*, 46(10), pp. 1695–1706, 2013.
<https://doi.org/10.1617/s11527-012-0008-y>
- [7] Wilson, D. M. "New Zealand pumice as a lightweight concrete aggregate", BSc Thesis, University of Canterbury, 1949.
- [8] del Coz-Díaz, J. J., Martínez-Martínez, J. E., Alonso-Martínez, M., Rabanal, F. P. Á. "Comparative study of LightWeight and Normal Concrete composite slabs behaviour under fire conditions", *Engineering Structures*, 207, 110196, 2020.
<https://doi.org/10.1016/j.engstruct.2020.110196>
- [9] Marzouk, H., Osman, M., Hussein, A. "Cyclic loading of high-strength lightweight concrete slabs", *ACI Structural Journal*, 98(2), pp. 207–214, 2001.
<https://doi.org/10.14359/10189>
- [10] Nainggolan, C. R., Wijatmiko, I., Wibowo, A. "Flexural behavior of reinforced concrete beam with polymer coated pumice", *AIP Conference Proceedings*, 1887, 020026, 2017.
<https://doi.org/10.1063/1.5003509>
- [11] Shafiq, P., Hassanpour, M., Razavi, S. V., Kobraei, M. "An investigation of the flexural behaviour of reinforced lightweight concrete beams", *International Journal of the Physical Sciences*, 6(10), pp. 2414–2421, 2011.
- [12] Sultan, M. A., Gaus, A., Hakim, R., Imran "Review of the flexural strength of lightweight concrete beam using pumice stone as of substitution partial coarse aggregate", *International Journal of GEOMATE*, 21(85), pp. 154–159, 2021.
<https://doi.org/10.21660/2021.85.j2184>
- [13] Suseno, H., Soehardjono, A., Wardana, I. N. G., Rachmansyah, A. "Performance of lightweight concrete one-way slabs using medium-K basaltic andesite pumice and scoria", *Asian Journal of Civil Engineering*, 19, pp. 473–485, 2018.
<https://doi.org/10.1007/s42107-018-0047-y>
- [14] Vimonsatit, V., Wahyuni, A., Nikraz, H. "Reinforced concrete beams with lightweight concrete infill", *Scientific Research and Essays*, 7(27), pp. 2370–2379, 2012.
<https://doi.org/10.5897/SRE12.115>
- [15] Wu, C.-H., Kan, Y.-C., Huang, C.-H., Yen, T., Chen, L.-H. "Flexural behavior and size effect of full scale reinforced lightweight concrete beam", *Journal of Marine Science and Technology*, 19(2), 4, 2011.
<https://doi.org/10.51400/2709-6998.2147>
- [16] Youm, K. S., Jeon, H. K., Park, Y. S., Lee, S. H., Moon, J. "Experimental study on punching shear of lightweight concrete slab", In: *Proceedings of the Thirteenth East Asia-Pacific Conference on Structural Engineering and Construction*, Sapporo, Japan, 2013, pp. E-6-4. [online] Available at: <http://hdl.handle.net/2115/54369>

- [17] Ahmed, I. M., Tsavdaridis, K. D. "Shear connection of prefabricated ultra-lightweight concrete slab systems (PUSSTM)", *Structures*, 36, pp. 65–97, 2022.
<https://doi.org/10.1016/j.istruc.2021.11.017>
- [18] Chung, J.-H., Bae, B.-I., Choi, H.-K., Jung, H.-S., Choi, C.-S. "Evaluation of punching shear strength of voided slabs considering the effect of the ratio b_0/d ", *Engineering Structures*, 164, pp. 70–81, 2018.
<https://doi.org/10.1016/j.engstruct.2018.02.085>
- [19] Chung, J.-H., Jung, H.-S., Bae, B.-I., Choi, C.-S., Choi, H.-K. "Two-way flexural behavior of donut-type voided slabs", *International Journal of Concrete Structures and Materials*, 12(1), 12, 2018.
<https://doi.org/10.1186/s40069-018-0247-6>
- [20] Chung, J.-H., Jung, H.-S., Choi, H.-K. "Flexural Strength and Stiffness of Donut-Type Voided Slab", *Applied Sciences*, 12(12), 5782, 2022.
<https://doi.org/10.3390/app12125782>
- [21] Albrecht, C., Albert, A., Pfeffer, K., Schnell, J. "Design and construction of two-way spanning reinforced concrete slabs with flattened rotationally symmetrical void formers", *Beton- und Stahlbetonbau*, 107(9), pp. 590–600, 2012. (in German)
<https://doi.org/10.1002/best.201200027>
- [22] Alfeehan, A. A., Abdulkareem, H. I., Mutashar, S. H. "Flexural behavior of sustainable reactive powder concrete bubbled slab flooring elements", *Challenge Journal of Structural Mechanics*, 3(2), pp. 81–89, 2017.
<https://doi.org/10.20528/cjsmec.2017.04.010>
- [23] Al-Gasham, T. S., Hilo, A. N., Alawsi, M. A. "Structural behavior of reinforced concrete one-way slabs voided by polystyrene balls", *Case Studies in Construction Materials*, 11, e00292, 2019.
<https://doi.org/10.1016/j.cscm.2019.e00292>
- [24] Fanella, D. A., Mahamid, M., Mota, M. "Flat plate-voided concrete slab systems: design, serviceability, fire resistance, and construction", *Practice Periodical on Structural Design and Construction*, 22(3), 04017004, 2017.
[https://doi.org/10.1061/\(ASCE\)SC.1943-5576.0000322](https://doi.org/10.1061/(ASCE)SC.1943-5576.0000322)
- [25] Ibrahim, A. M., Ali, N. K., Salman, W. D. "Finite element analysis of reinforced concrete slabs with spherical voids", *Diyala Journal of Engineering Sciences*, 6(4), pp. 15–37, 2013.
<https://doi.org/10.24237/djes.2013.06402>
- [26] Ibrahim, A. M., Ali, N. K., Salman, W. D. "Flexural capacities of reinforced concrete two-way bubbledeck slabs of plastic spherical voids", *Diyala Journal of Engineering Sciences*, 6, pp. 9–20, 2013.
<https://doi.org/10.24237/djes.2013.06202>
- [27] Khouzani, M. A., Zeynalian, M., Hashemi, M., Mostofinejad, D., Farahbod, F. "Study on shear behavior and capacity of biaxial ellipsoidal voided slabs", *Structures*, 27, pp. 1075–1085, 2020.
<https://doi.org/10.1016/j.istruc.2020.07.017>
- [28] Sagadevan, R., Rao, B. N. "Experimental and analytical investigation of punching shear capacity of biaxial voided slabs", *Structures*, 20, pp. 340–352, 2019.
<https://doi.org/10.1016/j.istruc.2019.03.013>
- [29] Al-Gasham, T. S., Mhalhal, J. M., Abid, S. R. "Quasi-static analysis of biaxial voided slabs with openings", *Structures*, 33, pp. 4176–4192, 2021.
<https://doi.org/10.1016/j.istruc.2021.07.021>
- [30] Daliform "U-Boot® Beton" [online] Available at: <https://www.daliform.com/en/disposable-formwork-for-two-way-lightened-voided-slabs/>
- [31] Taskin, K., Peker, K. "Design factors and the economical application of spherical type voids in RC slabs", In: *Proceedings of International Scientific Conference People, Buildings and Environment 2014 (PBE2014)*, Vol. 3., Kroměříž, Czech Republic, 2014, pp. 448–458. 2014. ISSN: 1805-6784
- [32] Khouzani, M. A., Zeynalian, M., Hashemi, M., Mostofinejad, D., Farahbod, F., Shahadifar, M. "A numerical study on flexural behavior of biaxial voided slabs containing steel cages", *Journal of Building Engineering*, 44, 103382, 2021.
<https://doi.org/10.1016/j.jobbe.2021.103382>
- [33] Valivonis, J., Skuturna, T., Daugevičius, M., Šneideris, A. "Punching shear strength of reinforced concrete slabs with plastic void formers", *Construction and Building Materials*, 145, pp. 518–527, 2017.
<https://doi.org/10.1016/j.conbuildmat.2017.04.057>
- [34] Kim, S. H. "Flexural Behavior of Void RC and PC Slab with Polystyrene Forms", *Key Engineering Materials*, 452–453, pp. 61–64, 2011.
<https://doi.org/10.4028/www.scientific.net/KEM.452-453.61>
- [35] Kim, S. H., Lee, K. K., Lee, H. S., Lee, K. J., Kang, I. S. "Bending and Shear Strength of I-Slab with Polystyrene Forms", *Key Engineering Materials*, 385–387, pp. 353–356, 2008.
<https://doi.org/10.4028/www.scientific.net/KEM.385-387.353>
- [36] Moeeni, M., Langroudi, J. R. "Tension stiffening in reinforced concrete hollow core slabs", *Asian Journal of Civil Engineering*, 23(5), 635–647, 2022.
<https://doi.org/10.1007/s42107-022-00445-9>
- [37] Ziverts, G. J. "A Study of Cardboard Voids for Prestressed Concrete Box Slabs", *PCI Journal*, 9(3), pp. 66–93, 1964.
<https://doi.org/10.15554/pcij.06011964.66.93>
- [38] Di Giacinto, D., Losanno, D., Ruocco, E., Grassia, L. "A Novel Steel-Concrete Composite Flooring System: Development and Preliminary Experimental Investigation", In: *Proceedings of the 4th World Congress on Civil, Structural, and Environmental Engineering (CSEE'19)*, Rome, Italy, 2019, Paper No. ICSECT 142. ISBN: 978-1-927877-52-4
<https://doi.org/10.11159/icsect19.142>
- [39] Kim, S. H. "Shear Strength of Void Slab with Polystyrene Forms", *Applied Mechanics and Materials*, 217, pp. 626–629, 2012.
<https://doi.org/10.4028/www.scientific.net/AMM.217-219.626>
- [40] Yardim, Y., Waleed, A. M. T., Saleh Jaafar, M. Laseima, S. "AAC-concrete lightweight precast composite floor slab", *Construction and Building Materials*, 40, pp. 405–410, 2013.
<https://doi.org/10.1016/j.conbuildmat.2012.10.011>
- [41] Jabir, H. A., Mhalhal, J. M., Al-Gasham, T. S. "Conventional and bubbled slab strips under limited repeated loads: A comparative experimental study", *Case Studies in Construction Materials*, 14, e00501, 2021.
<https://doi.org/10.1016/j.cscm.2021.e00501>
- [42] Allawi, A. A., Jabir, H. A. "Experimental behavior of laced reinforced concrete one way slab under static load", *Journal of Engineering*, 22(5), pp. 42–59, 2016. [online] Available at: <https://www.iasj.net/iasj/article/109423>

- [43] Wang, Y., Liu, H. T., Dou, G. F., Xi, C. H., Qian, L. "Experimental study of multi-ribbed one-way composite slabs made of steel fibre, foam, and normal concrete", *Archives of Civil Engineering*, 64(2), pp. 79–96, 2018.
<https://doi.org/10.2478/ace-2018-0018>
- [44] TSI "TS500-2000 Betonarme yapıların tasarım ve yapım kural-ları" (Design and Construction Rules of Reinforced Concrete Structures), Turkish Standards Institute, Ankara, Türkiye, 2000. (in Turkish)
- [45] Paunović, S., Šutanovac, A., Blagojević, P. "An alternative numerical model for fiber reinforced concrete strength evaluation", *Facta Universitatis, Series: Architecture and Civil Engineering*, 20(3), pp. 213–230, 2022.
<https://doi.org/10.2298/FUACE220223017P>
- [46] Vacev, T., Zorić, A., Grdić, D., Ristić, N., Grdić, Z., Milić, M. "Experimental and Numerical Analysis of Impact Strength of Concrete Slabs", *Periodica Polytechnica Civil Engineering*, 67(1), pp. 325–335, 2023.
<https://doi.org/10.3311/PPci.21084>
- [47] Simulia "ABAQUS 6.14 user's manuals", Dassault Systems Simulia Corporation, 2016. [online] Available at: <http://130.149.89.49:2080/v6.14/index.html>
- [48] Lubliner, J., Oliver, J., Oller, S., Oñate, E. "A plastic-damage model for concrete", *International Journal of Solids and Structures*, 25(3), pp. 299–326, 1989.
[https://doi.org/10.1016/0020-7683\(89\)90050-4](https://doi.org/10.1016/0020-7683(89)90050-4)
- [49] Wosatko, A., Winnicki, A., Polak, M. A., Pamin, J. "Role of dilata-tancy angle in plasticity-based models of concrete", *Archives of Civil and Mechanical Engineering*, 19, pp. 1268–1283, 2019.
<https://doi.org/10.1016/j.acme.2019.07.003>
- [50] Genikomsou, A. S., Polak, M. A. "Finite element analysis of punching shear of concrete slabs using damaged plasticity model in ABAQUS", *Engineering Structures*, 98, pp. 38–48, 2015.
<https://doi.org/10.1016/j.engstruct.2015.04.016>
- [51] Guo, L., Mao, R., Liu, Z., Li, S., Wu, G., Wang, Z. "Dynamic large deflection response of RC beams under low-speed impact loading", *Shock and Vibration*, 2020, 8812890, 2020.
<https://doi.org/10.1155/2020/8812890>
- [52] Hafezolghorani, M., Hejazi, F., Vaghei, R., Jaafar, M. S. B., Karimzade, K. "Simplified damage plasticity model for concrete", *Structural Engineering International*, 27(1), pp. 68–78. 2017.
<https://doi.org/10.2749/101686616X1081>
- [53] Rewers, I. "Numerical analysis of RC beam with high strength steel reinforcement using CDP model", *IOP Conference Series: Materials Science and Engineering*, 471(2), 022025, 2019.
<https://doi.org/10.1088/1757-899X/471/2/022025>
- [54] Kawamoto, Y., Stepan, J. "Analytical Study of Reinforced Concrete Slab Subjected to Soft Missile Impact", presented at Transactions, SMIRT-23, Conference on Structural Mechanics in Reactor Technology, Manchester, UK, Aug. 10–14, 2015.
- [55] Petrović, Ž., Milošević, B., Zorić, A., Ranković, S., Mladenović, B., Zlatkov, D. "Flexural Behavior of Continuous Beams Made of Self-Compacting Concrete (SCC)-Experimental and Numerical Analysis", *Applied Sciences*, 10(23), 8654, 2020.
<https://doi.org/10.3390/app10238654>
- [56] Demir, A., Ozturk, H., Edip, K., Stojmanovska, M., Bogdanovic, A. "Effect of viscosity parameter on the numerical simulation of rein-forced concrete deep beam behavior", [pdf] *The Online Journal of Science and Technology*, 8(3), pp. 50-56, 2018. Available at: <https://www.tojsat.net/journals/tojsat/articles/v08i03/v08i03-09.pdf>
- [57] Chinese Code "GB 50010-2010 Code for Design of Concrete Structures", Ministry of Housing and Urban-Rural Development of the People's Republic of China, Beijing, China, 2010.
- [58] TSI "TS ISO 9194 Yapıların projelendirilme esasları-taşıyıcı olan ve olmayan elemanlar depolanmış malzemeler-yoğunluk" (Designing Principles of Buildings-Bearing and Non-Bearing Elements), Ankara, Turkish Standards Institute, Ankara, Türkiye, 1997. (in Turkish)
- [59] "RBT 2019 Riskli yapıların tespit edilmesine ilişkin esaslar" (Ministry of Environment and Urbanization "Principles Regarding Detection of Risky Structures), Environment and Urban Ministry, Ankara, Türkiye, 2019. (in Turkish)
- [60] CEN "Eurocode 2. Design of Concrete Structures", European Committee for Standardization, Brussels, Belgium, 2004.
- [61] TSI "TEC-2018 Türkiye bina deprem yönetmeliği" (Turkey Building Earthquake Regulation), Environment and Urban Ministry, Ankara, Türkiye, 2018. (in Turkish)
- [62] TSI "TS 708 Çelik-Betonarme için-Donatı çeliği" (Steel for rein-forced concrete - reinforcing steel), Turkish Standards Institute, Ankara, Türkiye, 2010. (in Turkish)
- [63] Ersoy, U., Özcebe, G., Canbay, E. "Reinforced Concrete Volume 1-Principles of Conduct and Calculation", Evrim Yayınları, 2019. ISBN: 9789755032399
- [64] Marais, C. C. "Design adjustment factors and the economical application of concrete flat-slabs with internal spherical voids in South Africa", Doctoral Dissertation, University of Pretoria, 2010. [online] Available at: <http://hdl.handle.net/2263/27476>
- [65] Subramanian, K., Bhuvaneshwari, P., Jabez, N. A. "Flexural behaviour of biaxial slabs voided with spherical HDPP void formers", *Iranian Journal of Science and Technology, Transactions of Civil Engineering*, 41, pp. 373–381, 2017.
<https://doi.org/10.1007/s40996-017-0077-9>
- [66] ACI "ACI318RM-19 Building Code Requirements for Structural Concrete and Commentary (ACI, American Concrete Institute)", American Concrete Institute, Farmington Hills, MI, USA, 2019.
- [67] Lee, C.-H., Mansouri, I., Bae, J., Ryu, J. "Current and New Approaches to Predict the Deflections of One-Way Flexural Members with a Focus on Composite Steel Deck Slabs Voided by Circular Tubes", *Materials*, 14(2), 421, 2021.
<https://doi.org/10.3390/ma14020421>